Cold sensitivity of the SARS-CoV-2 spike ectodomain

Robert J Edwards[1,2‡,*], Katayoun Mansouri[1,‡], Victoria Stalls[1,‡], Kartik Manne[1,‡], Brian Watts[1], Rob Parks[1], Katarzyna Janowska[1], Sophie M. C. Gobeil[1], Dapeng Li[1], Xiaozhi Lu[1], Margaret Deyton[1], Jordan Sprenz[1], Wilton Williams[1,2], Kevin Saunders[1,3], Gregory D. Sempowski[1], Rory Henderson[1,2], Munir Alam[1,2], Barton F. Haynes[1,2], Priyamvada Acharya[1,3,*]

Affiliations:
[1] Duke Human Vaccine Institute, Durham NC 27710, USA
[2] Duke University, Department of Medicine, Durham NC 27710, USA
[3] Duke University, Department of Surgery, Durham NC 27710, USA
[4] Duke University, Department of Immunology, Durham NC 27710, USA
‡These authors contributed equally.
*To whom correspondence should be addressed

Correspondence to: Robert J Edwards (rj.edwards@duke.edu) and Priyamvada Acharya (priyamvada.acharya@duke.edu)

Abstract

The SARS-CoV-2 spike (S) protein, a primary target for COVID-19 vaccine development, presents two conformations of its Receptor Binding Domain - a receptor-accessible “up” conformation, or a receptor-inaccessible “down” conformation. Here, we report unexpected cold sensitivity of a commonly used S ectodomain construct, and resolution of this cold sensitivity in a “down” state stabilized spike. Our results will impact structural, functional and vaccine studies that use the SARS-CoV-2 S ectodomain.

The spike (S) protein of SARS-CoV-2 mediates receptor binding and cell entry and is a key target for vaccine development efforts. Stabilized S ectodomain constructs have been developed that mimic the native spike, bind ACE-2 receptor (*1, 2*), and present epitopes for neutralizing antibodies on their surface (*3-6*). The S ectodomain construct discussed here (Figure 1A), and other similar constructs, are being widely used for structural biology and vaccine studies (*1-3, 7, 8*). Purified S ectodomain proteins (*9*) are assessed by SDS-PAGE, size exclusion chromatography (SEC), differential scanning fluorimetry (DSF) (*10*), and negative stain electron microscopy (NSEM) (Figure 1B-G and Extended Data Figure 1) for quality control. NSEM proved especially important because it reveals the three-dimensional integrity of individual molecules, allowing us to discriminate between preparations that otherwise looked similar by bulk measures such as SDS-PAGE and SEC (Extended Data Figure 1). The variability between preparations suggested a fragile S ectodomain. Indeed, such fragility and measures to overcome have been previously reported (*11, 12*). We traced the apparent spike fragility to rapid deterioration upon storage at 4 °C (Figure 1 B-E), and hypothesized that the stabilized SARS-CoV-2 S ectodomain is a cold-sensitive protein.

We tracked the behavior of the S ectodomain stored under different conditions (Figure 1, Extended Data Figures 2-6). NSEM results are summarized in Figure 1E. Freshly prepared spike samples showed 75% well-formed spikes on average. Spike fraction was slightly decreased to 64% by one cycle of freeze/thaw and to 59% by storage at room temperature for up to one week; whereas it was slightly increased to 83% by 1-week storage at 37 °C. Storage at 4 °C, in a buffer containing 20 Tris.HCl, pH 8.0 and 200 mM NaCl, caused a significant decrease to only 5% intact spike. We also found that well-formed spike could be recovered after cold-storage with a 3-hour incubation at 37 °C (Figure 1D-E). Longer incubations at 37 °C yielded no further improvement (Figure 1E) and showed slight aggregation. Similar to our NSEM

results, we also see substantial differences in the quality and dispersion of protein in cryo-EM grids depending on how the specimen was stored (Extended Data Figure 6).

The S ectodomain was recently reported to exhibit conformational changes with pH (*12*), so we questioned whether the spike degradation we observed was due to the expected temperature-dependent pH change for Tris buffer (*13*). We split a spike preparation and SEC-purified one fraction into Tris buffer pH 8.0, and the other into MOPS buffer pH 7.4, which is expected to change only slightly to pH 7.42 at 4 °C, due its smaller temperature dependence compared to Tris (*13*) . Room-temperature storage for one week at pH 8.0 (Tris buffer) reduced the spike fraction to 50% (Figure 1E), similar to the average of 59% after room-temperature storage. In contrast, cold-storage at pH 7.42 (MOPS buffer) reduced the spike fraction to 4%, similar to the average of 5% for cold-storage in Tris buffer. Thus, the primary cause of spike degradation here appears to be the temperature change and not the pH shift. Incubating the spike at 4 °C in MES, pH 6 buffer reduced but did not eliminate the cold-sensitivity.

We next demonstrate that the observed cold-sensitivity is not merely an artifact of the negative stain sample preparation but is a property of the bulk protein in solution. First, we measured stability with DSF (*10*), and observed distinct profile shifts indicating lower stability when spike samples were stored at 4 °C (Figures 1 F). Next, we performed differential scanning calorimetry (DSC) to obtain quantitative measures of the melting temperatures, T_m (Figure 1G and Extended Data Figure 3). After one week of storage at 37 °C, the spike sample demonstrated an asymmetric unfolding transition with a T_m of 65.5 °C. After sample storage at 22 °C for one week, we observed a second low-T_m transition at 48.2 °C. After sample storage at 4°C for one week, we observed a similar two-peak profile with a markedly more pronounced low-T_m transition (T_m = 48.4 °C). Upon returning the 4 °C sample to 37 °C for 3 hours prior to analysis, we observed an amplitude reduction of the low-T_m transition (T_m = 49.2 °C) and a corresponding amplitude increase in the high-T_m transition (T_m = 66.0 °C). The DSC results

confirmed that storage at 4 °C destabilizes the spike compared to samples stored at 22 °C or 37 °C, and that returning the destabilized spike to 37 °C for 3 hours substantially restores its stability.

We next tested the effects of cold-induced instability on antibody and receptor binding by SPR and ELISA (Figures 1H and Extended Data Figure 4-5). We found that spike stored at 4 °C showed higher binding to ACE-2 and antibody CR3022, both of which require an "up" RBD conformation (*1, 9, 12*). In contrast, cold-storage reduced binding to antibody 2G12, suggesting disruption of the 2G12 quaternary glycan epitope in the S2 subunit (*14*), upon cold-storage. We also tested two antibodies isolated from a COVID-19 convalescent patient (Extended Data Figure 4), one mapped to the ACE-2 binding site, AB712199, and another mapped to the S2 region of the spike, AB511584. Both antibodies showed differential binding depending on how the spike was stored, highlighting the importance of accounting for this cold-sensitive behavior of the S ectodomain for routine serology assays.

Because our results suggested that cold-induced destabilization was associated with increased RBD-exposure of the S ectodomain, we asked whether a "down" state stabilized S ectodomain might be resistant to cold-induced denaturation. We screened a panel of differentially stabilized S mutants (Figure 2) that included a new variant that combined the recently described rS2d (*9*) and HexaPro mutations (*11*). This new variant, named rS2d-HexaPro, showed substantial increase in production yields of the all-RBD-down spike (Figure 2C-E, Extended Data Figure 7 and Supplementary Movie 1). We also included in the NSEM screen two glycan-deleted mutants, 2P-N165A and 2P-N234A (*15*), that favor the RBD "up" or "down" conformation, respectively (Figure 2F). While both glycan-deleted mutants showed substantial reduction of spike percentage after incubation at 4 °C (Figure 2F), both HexaPro and rS2d-HexaPro appeared more resistant to cold-induced denaturation, with the rS2d-HexaPro sample showing a higher spike percentage than HexaPro. Thermostability and binding studies

(Figures 2G-H) further confirmed that both HexaPro and rS2d-HexaPro were more resistant to cold destabilization compared to the 2P version (Figure 1). ACE-2 binding was knocked down for the rS2d-HexaPro for all temperatures, as expected for a spike fixed in an RBD-down conformation, while ACE-2 binding was increased for HexaPro after incubation at 4 °C compared to the levels obtained in the 37 °C incubated samples showing that the HexaPro structure remained susceptible to perturbation at lower temperatures, albeit less so than the 2P version.

Overall, our results demonstrate the cold-sensitivity of the furin-cleavage deficient SARS-CoV-2 ectodomain, and its impact on antibody and receptor binding. We have also shown that this cold destabilization is substantially reduced in the HexaPro spike and further reduced by stabilization of the S ectodomain in a disulfide-locked “down” position.

Acknowledgements

This work was supported by NIH NIAID extramural project grants R01 AI145687 (P.A.), and AI058607 (G.S.), funding from the Department of Defense HR0011-17-2-0069 (G.S.) and a contract from the State of North Carolina Pandemic Recovery Office through funds from the Coronavirus Aid, Relief, and Economic Security (CARES) Act (B.F.H.). This work utilized the DSC platform supported by the Duke Consortia for HIV/AIDS Vaccine Development (CHAVD) and the Titan Krios microscope in the Shared Materials and Instrumentation Facility at Duke University.

Author contributions

R.J.E., K.Mansouri., V.S. and P.A. discovered the effect of storage temperature on spike stability. R.J.E. led NSEM studies and established quantitative metrics for spike QC. K.Mansouri collected NSEM data and performed analyses. V.S. purified proteins and performed thermostability measurements. K.Manne purified proteins, performed SPR assays, prepared

141 samples for NSEM, Tycho, ELISA, SPR and DSC measurements, and coordinated the study
142 between the different research teams. B.W. performed DSC measurements. R.P. and M.D.
143 performed ELISA assays. D.L., X.L., K.S. and G.S. isolated antibodies from convalescent
144 patient. S.G. and K. J. purified proteins and performed thermostability assays. W.W. performed
145 ELISA assays. R.H. initiated the DSC experiments and provided the rS2d, 2P-N234A and 2P-
146 N165A constructs prior to publication. M.A. supervised the DSC experiments. B.F.H. supervised
147 ELISA experiments and antibody isolation. P.A. oversaw and led the study, and co-wrote the
148 paper with R.J.E. and V.S. All authors reviewed and commented on the manuscript.

149

Methods

Protein expression and purification

SARS-CoV-2 ectodomain constructs were produced and purified (*1, 11*) as follows. A gene encoding residues 1−1208 of the SARS-CoV-2 S (GenBank: MN908947) with proline substitutions at residues 986 and 987, a “GSAS” substitution at the furin cleavage site (residues 682–685), a C-terminal T4 fibritin trimerization motif, an HRV3C protease cleavage site, a TwinStrepTag and an 8XHisTag was synthesized and cloned into the mammalian expression vector pαH. Plasmids were transiently transfected into either FreeStyle-293F cells or CHO cells using Turbo293 (SpeedBiosystems) or ExpiFectamine CHO Transfection Kit (ThermoFisher), respectively. Protein was purified on the sixth day post-transfection from filtered supernatant using StrepTactin resin (IBA), followed by SEC purification using a Superose 6 10/300 Increase column in nCoV buffer (2mM Tris, pH 8.0, 200 mM NaCl, 0.02% sodium azide).

Antibodies were produced in Expi293 cells and purified by Protein A affinity. For ACE-2 constructs, the ACE-2 C-terminus was fused with either the human or mouse Fc region including C-terminal 6X His-tag on the Fc domain. ACE-2 with human Fc tag was purified by Protein A affinity chromatography, and ACE-2 with mouse F_C tag was purified by Ni-NTA chromatography.

Negative-stain electron microscopy

Spike samples were pre-incubated (stored) for specified times in nCoV buffer at 4, 22 or 37 °C, then moved to room temperature for preparation of NSEM grids, which was complete in less than 5 min. Samples were diluted to 100 µg/ml with room-temperature buffer containing 20 mM HEPES pH 7.4, 150 mM NaCl, 5% glycerol and 7.5 mM glutaraldehyde, and incubated 5 min; then glutaraldehyde was quenched for 5 min by addition of 1M Tris stock to a final concentration of 75 mM. A 5-µl drop of sample was applied to a glow-discharged, carbon-coated grid for 10-15

s, blotted, stained with 2% uranyl formate, blotted and air-dried. Images were obtained with a Philips EM420 electron microscope at 120 kV, 82,000× magnification, and a 4.02 Å pixel size. The RELION program (*16*) was used for particle picking, 2D and 3D class averaging.

Thermostability assays

Thermostability of the S ectodomain samples were measured using DSF and DSC. Samples were purified and buffer exchanged into HBS buffer (10 mM HEPES, 150 mM NaCl, pH 7.4) by SEC on a Superose 6 10/300 column. DSF assay was performed using Tycho NT. 6 (NanoTemper Technologies). Spike variants were diluted (0.15 mg/ml) in HBS and run in triplicate. Intrinsic fluorescence was recorded at 330 nm and 350 nm while heating the sample from 35–95 °C at a rate of 30 °C/min. The ratio of fluorescence (350/330 nm) and inflection temperatures (Ti) were calculated by Tycho NT. 6.

DSC measurements were performed using the NanoDSC platform (TA instruments; New Castle, DE) on samples freshly purified by SEC (Figure S1), diluted to 0.2–0.3 mg/mL in HBS, and degassed for 15 min at room temperature prior to analysis. DSC cells were conditioned with filtered, degassed HBS prior to sample loading. Protein samples were heated from 10 °C to 100 °C at 1 °C/min under 3 atm pressure using HBS as the reference buffer. The observed denaturation profiles were buffer subtracted, converted to molar heat capacity, baseline-corrected with a 6th-order polynomial, and fit with 2-4 Gaussian transition models, as needed, using the NanoAnalyze software (TA Instruments). The peak transition temperature (T_m) is reported as the temperature at the maximum observed heat capacity of each transition peak.

Isolation of antibodies from convalescent patients

Human SARS-CoV-2 Spike antibodies Ab712199 and Ab511584 were isolated from a COVID-19 convalescent individual. Briefly, PBMC samples collected after the onset of the symptoms

were stained and the memory B cells were sorted with SARS-CoV-2 Spike-2p probes. Antibody IgH and IgK/L genes were recovered from the single-cell sorted cells, cloned into human IgG1 constant region backbone, and purified by Protein A beads as previously described (*17*).

ELISA assays

Spike samples were pre-incubated at different temperatures then tested for antibody- or ACE-2-binding in ELISA assays as previously described (*18, 19*). Assays were run in two formats. In the first format antibodies or ACE-2 protein were coated on 384-well plates at 2 µg/ml overnight at 4°C, washed, blocked and followed by two-fold serially diluted spike protein starting at 25 µg/ml. Binding was detected with polyclonal anti-SARS-CoV-2 spike rabbit serum (developed in our lab), followed by goat anti-rabbit-HRP (Abcam #ab97080) and TMB substrate (Sera Care Life Sciences #5120-0083). Absorbance was read at 450 nm. In the second format, serially diluted spike protein was bound in individual wells of 384-well plates, which were previously coated with streptavidin (Thermo Fisher Scientific #S-888) at 2 µg/ml and blocked. Proteins were incubated and washed, then human mAbs were added at 10 µg/ml. Antibodies were incubated, washed and binding detected with goat anti-human-HRP (Jackson ImmunoResearch Laboratories, #109-035-098) and TMB substrate.

Commercially obtained constructs of SARS-CoV-2 spike ectodomain (S1+S2 ECD, S2 ECD and RBD) (Sino Biological Inc cat# 40589-V08B1 and 40590-V08B respectively and RBD from Genescript cat# Z03483) were coated directly on 384-well plates at 2 µg/ml and incubated overnight at 4 °C. Plates were washed, blocked and human mAbs three-fold serially diluted from 100 µg/ml were added for 1 hour at room temp followed by washing. Binding was detected with Goat anti-human IgG-HRP followed by TMB substrate.

Surface Plasmon Resonance

Antibody binding to SARS-CoV-2 spike constructs was assessed by surface plasmon resonance on a Biacore T-200 (GE-Healthcare) at 25°C with HBS buffer with 3 mM EDTA and 0.05% surfactant P-20 added. Antibodies captured on a CM5 chip coated with amine-coupled human Anti-Fc (8000RU) were assayed by SARS-CoV-2 spike at 200 nM. The surface was regenerated between injections with 3 M $MgCl_2$ solution for 10 s at 100 µl/min. Sensorgram data were analyzed using the BiaEvaluation software (GE Healthcare).

Cryo-EM

Purified SARS-CoV-2 spike preparations were diluted to a concentration of ~1 mg/mL in 2 mM Tris pH 8.0, 200 mM NaCl and 0.02% NaN_3. A 2.5-µL drop of protein was deposited on a CF-1.2/1.3 grid that had been glow discharged for 30 seconds in a PELCO easiGlow™ Glow Discharge Cleaning System. After a 30 s incubation in >95% humidity, excess protein was blotted away for 2.5 seconds before being plunge frozen into liquid ethane using a Leica EM GP2 plunge freezer (Leica Microsystems). Frozen grids were imaged in a Titan Krios (Thermo Fisher) equipped with a K3 detector (Gatan).

Data Availability

The datasets generated the current study are available from the corresponding author on reasonable request.

References

1. D. Wrapp *et al.*, Cryo-EM structure of the 2019-nCoV spike in the prefusion conformation. *Science* **367**, 1260-1263 (2020).
2. A. C. Walls *et al.*, Structure, Function, and Antigenicity of the SARS-CoV-2 Spike Glycoprotein. *Cell* **181**, 281-292 e286 (2020).
3. C. O. Barnes *et al.*, Structures of human antibodies bound to SARS-CoV-2 spike reveal common epitopes and recurrent features of antibodies. *bioRxiv*, (2020).
4. D. Pinto *et al.*, Cross-neutralization of SARS-CoV-2 by a human monoclonal SARS-CoV antibody. *Nature*, (2020).
5. C. E. Mire *et al.*, A Cross-Reactive Humanized Monoclonal Antibody Targeting Fusion Glycoprotein Function Protects Ferrets Against Lethal Nipah Virus and Hendra Virus Infection. *J Infect Dis* **221**, S471-S479 (2020).
6. Z. Ke, Oton, J.; Qu, K.; Cortese, M.; Zila, V.; McKeane, L.; Nakane, T.; Zivanov, J.; Neufeldt, C.J.; Lu, J.M.; Peukes, J.; Xiong, X.; Krausslich, H.G.; Scheres, S.H.W.; Bartenschlager, R.; Briggs, J.A.G., Structures, conformations and distributions of SARS-CoV-2 spike protein trimers on intact virions. *bioRxiv*, (2020).
7. L. Liu *et al.*, Potent Neutralizing Monoclonal Antibodies Directed to Multiple Epitopes on the SARS-CoV-2 Spike. *bioRxiv*, (2020).
8. T. Zhou *et al.*, Structure-Based Design with Tag-Based Purification and In-Process Biotinylation Enable Streamlined Development of SARS-CoV-2 Spike Molecular Probes. *bioRxiv*, (2020).
9. R. Henderson *et al.*, Controlling the SARS-CoV-2 spike glycoprotein conformation. *Nat Struct Mol Biol*, (2020).
10. A. O. Magnusson *et al.*, nanoDSF as screening tool for enzyme libraries and biotechnology development. *FEBS J* **286**, 184-204 (2019).
11. C. L. Hsieh *et al.*, Structure-based design of prefusion-stabilized SARS-CoV-2 spikes. *Science*, (2020).
12. T. Zhou *et al.*, A pH-dependent switch mediates conformational masking of SARS-CoV-2 spike. *bioRxiv*, (2020).
13. N. E. Good *et al.*, Hydrogen ion buffers for biological research. *Biochemistry* **5**, 467-477 (1966).
14. P. Acharya *et al.*, A glycan cluster on the SARS-CoV-2 spike ectodomain is recognized by Fab-dimerized glycan-reactive antibodies. *bioRxiv*, (2020).
15. R. Henderson *et al.*, Glycans on the SARS-CoV-2 Spike Control the Receptor Binding Domain Conformation. *bioRxiv*, (2020).
16. S. H. W. Scheres, in *Methods in Enzymology,* R. A. Crowther, Ed. (Academic Press, 2016), vol. 579, pp. 125-157.
17. H. X. Liao *et al.*, Co-evolution of a broadly neutralizing HIV-1 antibody and founder virus. *Nature* **496**, 469-476 (2013).
18. S. M. Alam *et al.*, Mimicry of an HIV broadly neutralizing antibody epitope with a synthetic glycopeptide. *Science translational medicine* **9**, (2017).
19. M. Bonsignori *et al.*, Staged induction of HIV-1 glycan-dependent broadly neutralizing antibodies. *Science translational medicine* **9**, (2017).

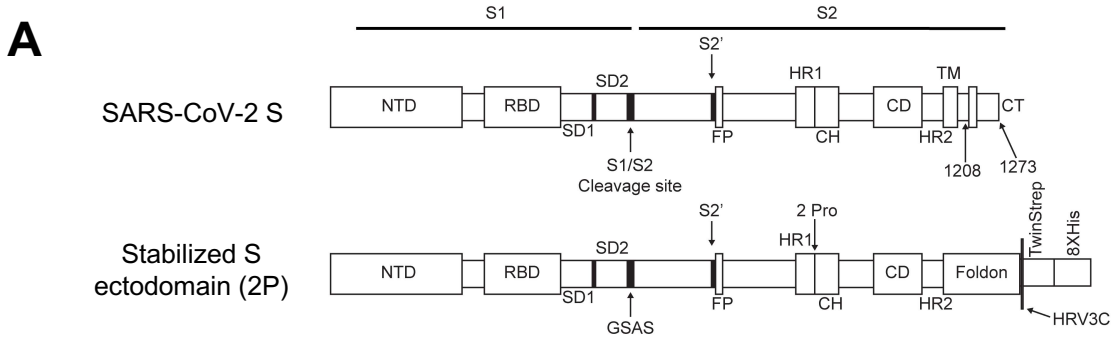

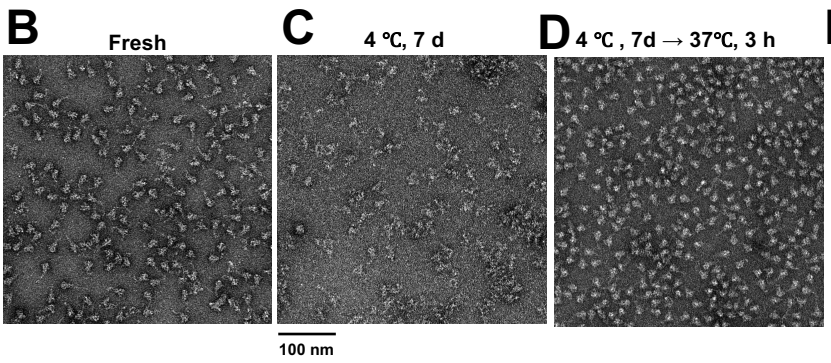

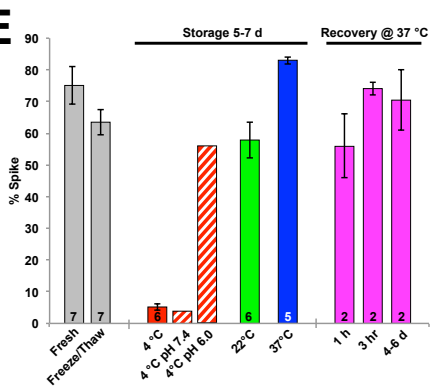

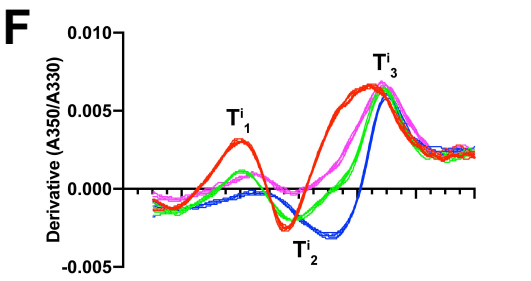

Storage Temperature	T^i_1	T^i_2	T^i_3
37 °C	53.7 ± 1.1	65 ± 0.2	74.8 ± 0.2
22 °C	49.9 ± 0.2	58.6 ± 0.3	74.2 ± 0.2
4 °C	49.9 ± 0.4	57.5 ± 0.3	71.9 ± 0.2
4->37 °C Recovery	52.2 ± 0.5	58.8 ± 0.5	74.1 ± 0.3

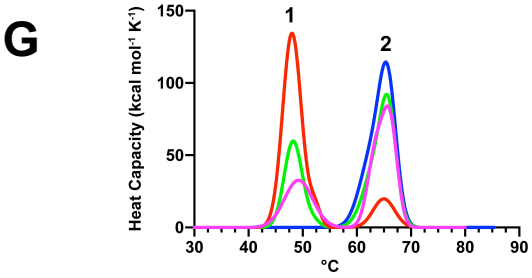

Storage Temperature	Transition Peak 1 T_m (°C)	Transition Peak 2 T_m (°C)
37 °C	N/A	65.5 ± 0.1
22 °C	48.23 ± 0.04	65.8 ± 0.1
4 °C	48.41 ± 0.01	65.1 ± 0.2
4->37 °C Recovery	49.21 ± 0.05	65.95 ± 0.01

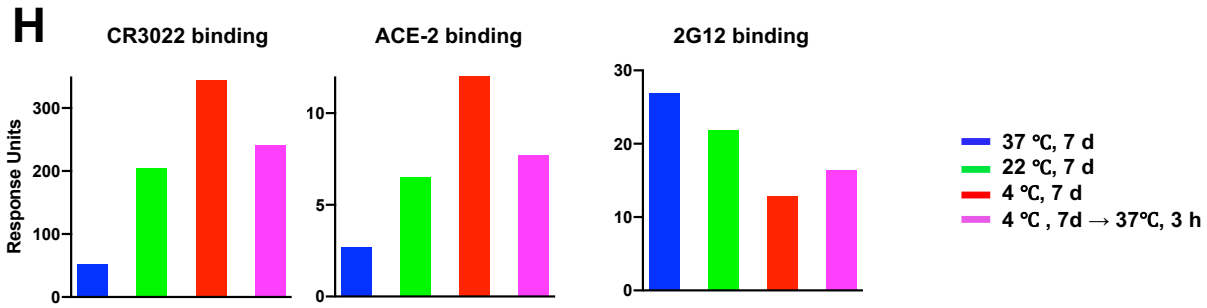

Figure 1. Temperature-dependence of the SARS-CoV-2 S ectodomain. (A) Schematic of the SARS-CoV-2 spike (top) and a furin cleavage-deficient, soluble, stabilized ectodomain construct (bottom). **(B-D)** Representative NSEM micrograph from **(B)** a freshly prepared sample of the S ectodomain, **(C)** the same sample after storing the protein for one week at 4 °C, **(D)** the same sample after storing the protein for one week at 4 °C followed by a 3-hour incubation at 37 °C. **(E)** Bar graph summarizing NSEM results on S ectodomain samples stored under different conditions. From left to right, bars show spike percentage in a fresh sample of spike; after the spike undergoes a single freeze-thaw cycle; after it has been incubated for 5-7 days at 4 °C (red), 22 °C (green) or 37 °C (blue); and spike samples that were stored for 1 week at 4 °C, then incubated at 37 °C for 1 hour, 3 hours, or 4-6 days. Solid bars indicate averages, with error bars indicating standard error of the mean and the number of samples indicated at the bottom of each column. Hatched bars represent measurements from a single sample. **(F)** *(top)* DSF profiles obtained by following changes in intrinsic fluorescence upon applying a thermal ramp to the sample and expressed as the first derivative of the ratio between fluorescence at 350 nm and 330 nm. Maxima and minima indicate inflection temperatures, T^i. *(bottom)* Table of inflection temperatures, expressed as averages ± standard deviation, N=5. **(G)** *(top)* DSC profiles. *(bottom)* Table of melting temperatures, T_m, with values expressed as averages ± standard deviation, N=2. **(H)** Antibody CR3022 IgG (left), ACE-2 (middle) and 2G12 IgG (right) binding to spike stored at different temperatures measured by SPR. Data for spike samples measured after a 1-week incubation at 37, 22, and 4 °C, are shown in blue, green, and red respectively; sample stored 1 week at 4 °C and then incubated for 3 hours at 37 °C shown in magenta.

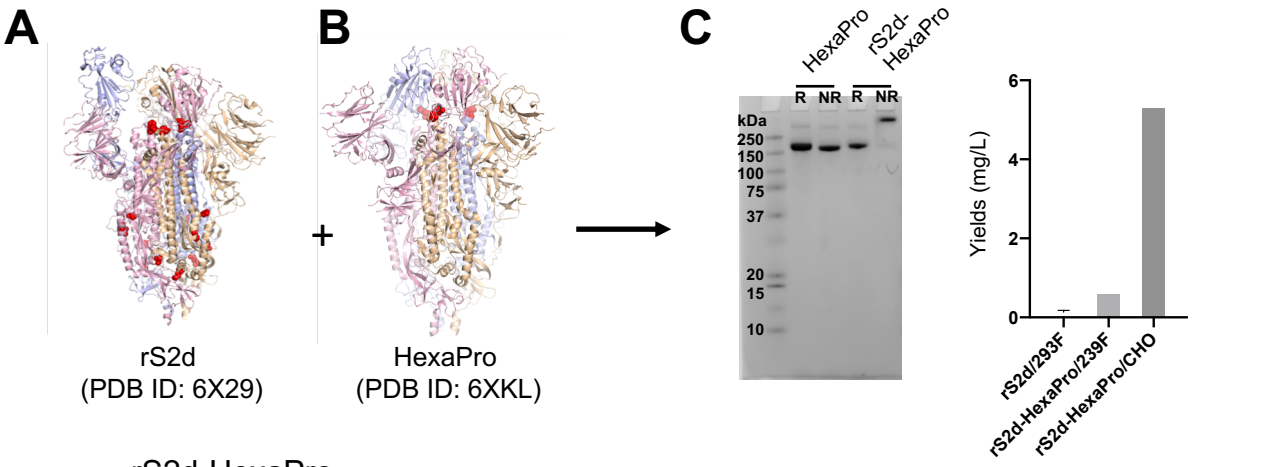
A
B
C
rS2d
(PDB ID: 6X29)
HexaPro
(PDB ID: 6XKL)
HexaPro
rS2d-HexaPro
R NR R NR
kDa
250
150
100
75
37
20
15
10
Yields (mg/L)
rS2d/293F
rS2d-HexaPro/239F
rS2d-HexaPro/CHO

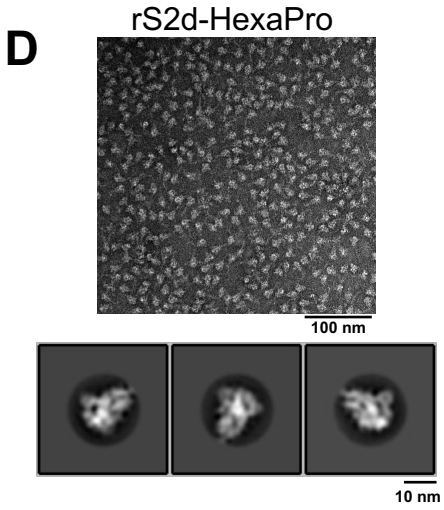
D
rS2d-HexaPro
100 nm
10 nm

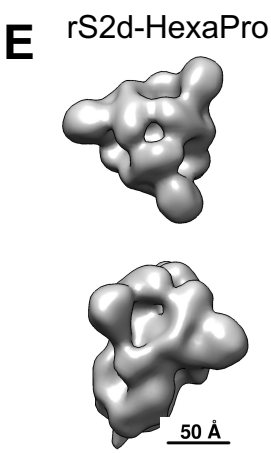
E
rS2d-HexaPro
50 Å

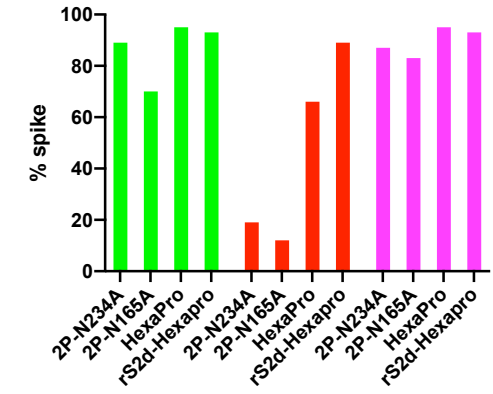
F
% spike
2P-N234A
2P-N165A
HexaPro
rS2d-Hexapro

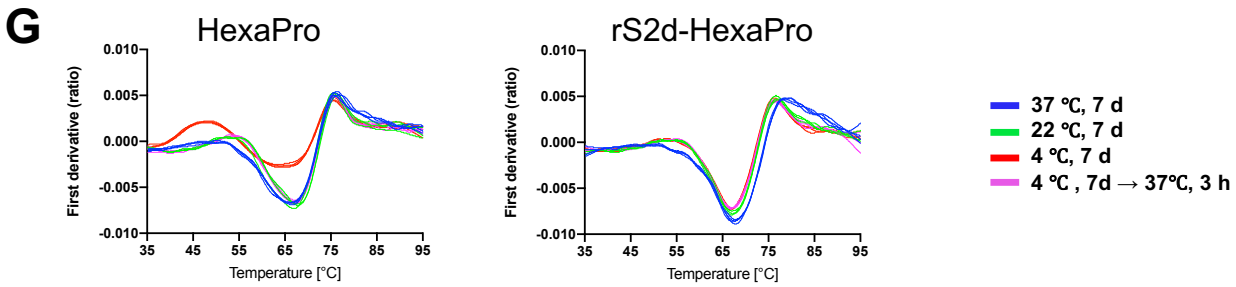
G
HexaPro
rS2d-HexaPro
First derivative (ratio)
Temperature [°C]
37 ℃, 7 d
22 ℃, 7 d
4 ℃, 7 d
4 ℃ , 7d → 37℃, 3 h

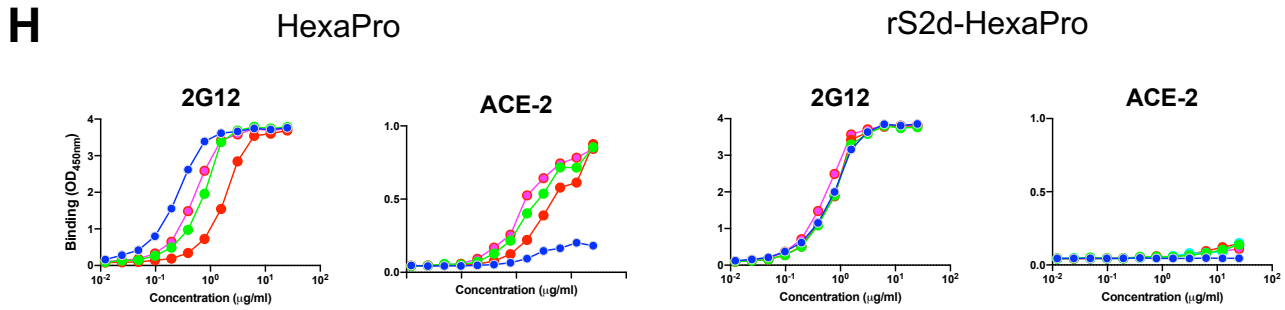
H
HexaPro
rS2d-HexaPro
2G12
ACE-2
Binding (OD450nm)
Concentration (μg/ml)

Figure 2. Engineered SARS-CoV-2 spike variant, rS2d-HexaPro, is resistant to temperature-dependent structural changes. (A-B) Structures of **(A)** HexaPro showing a 1-RBD-up conformation (PDB ID: 6X29) and **(B)** rS2d (PDB ID: 6XKL) showing a all-RBD-down conformation. **(C)** *(left)* SDS-PAGE. Lane 1: Molecular weight marker, Lanes 2 and 3: HexaPro, Lane 4 and 5: rS2d-HexaPro. R= Reducing, and NR = Non-reducing conditions. *(right)* Bar graph summarizing protein yields in mg/L of culture for, from left to right, rS2d produced in 293F cells, rS2d-HexaPro produced in Freestyle 293F cells, and rS2d-HexaPro expressed in CHO cells. **(D)** *(top)* Representative NSEM micrograph from a preparation of rS2d-Hexapro and *(bottom)* 2D class averages. **(E)** 3D reconstruction of rS2d-Hexapro obtained from NSEM data. **(F)** Bar graph summarizing results from NSEM on spike variants stored at different temperatures **(G)** DSF profiles for Hexapro (left) and rS2d-Hexapro (right). **(H)** Binding of 2G12 and ACE-2 to Hexapro (left) and rS2d-Hexapro (right) measured by ELISA. Serially diluted spike protein was bound in individual wells of 384-well plates, which were previously coated with streptavidin. Proteins were incubated and washed, then 2G12 at 10 µg/ml or ACE-2 with a mouse Fc tag at 2 µg/ml were added. Antibodies were incubated, washed and binding detected with goat anti-human-HRP.

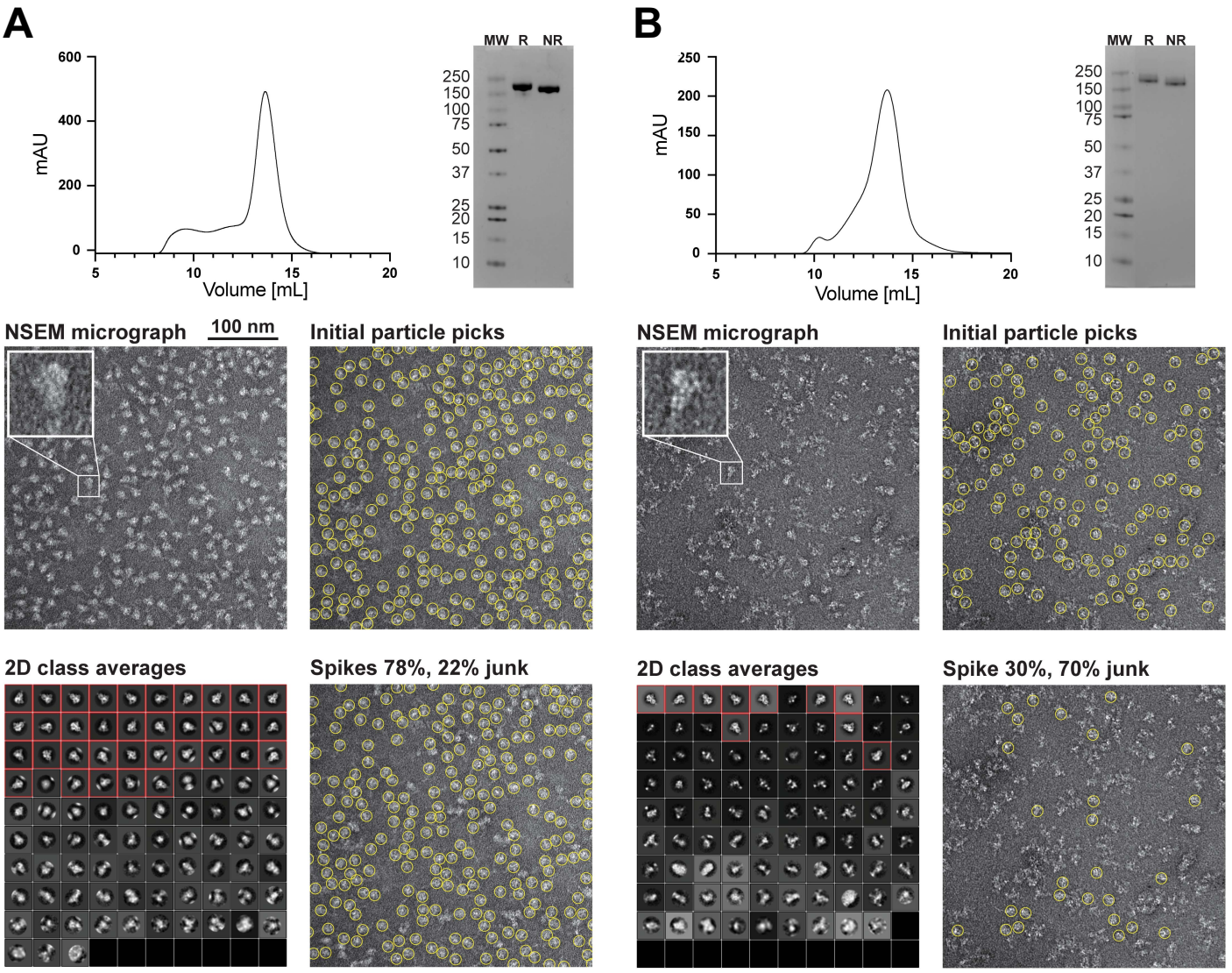

Extended Data Figure 1. Purification and quality control of the SARS-CoV-2 S protein ectodomain. (A and B) Two representative spike preparations that together highlight the role of NSEM in discriminating between good **(A)** and bad **(B)** spike preparations that otherwise appear to be of similar quality by SEC (top, left) and SDS-PAGE (top, right). Representative micrographs from each prep are shown, middle left. Protein appears as white blobs on gray background. Insets show a single kite-shaped spike particle enlarged. At the middle right, automatic particle picking is shown as yellow circles superimposed on the micrograph. Sets of ~20,000 initial particles picks are subjected to automated 2D classification to group together and average particles with similar features into discrete classes, bottom left. In the 2D class averages for each sample, the classes that contain the SARS-Cov-2 S ectodomain (shown within red boxes) can be clearly distinguished from classes that contain junk. The final spike picks come from the particles contained within the indicated classes and their total number provide an estimate of the ratio between the SARS-CoV-2 S ectodomain and junk seen in the NSEM sample.

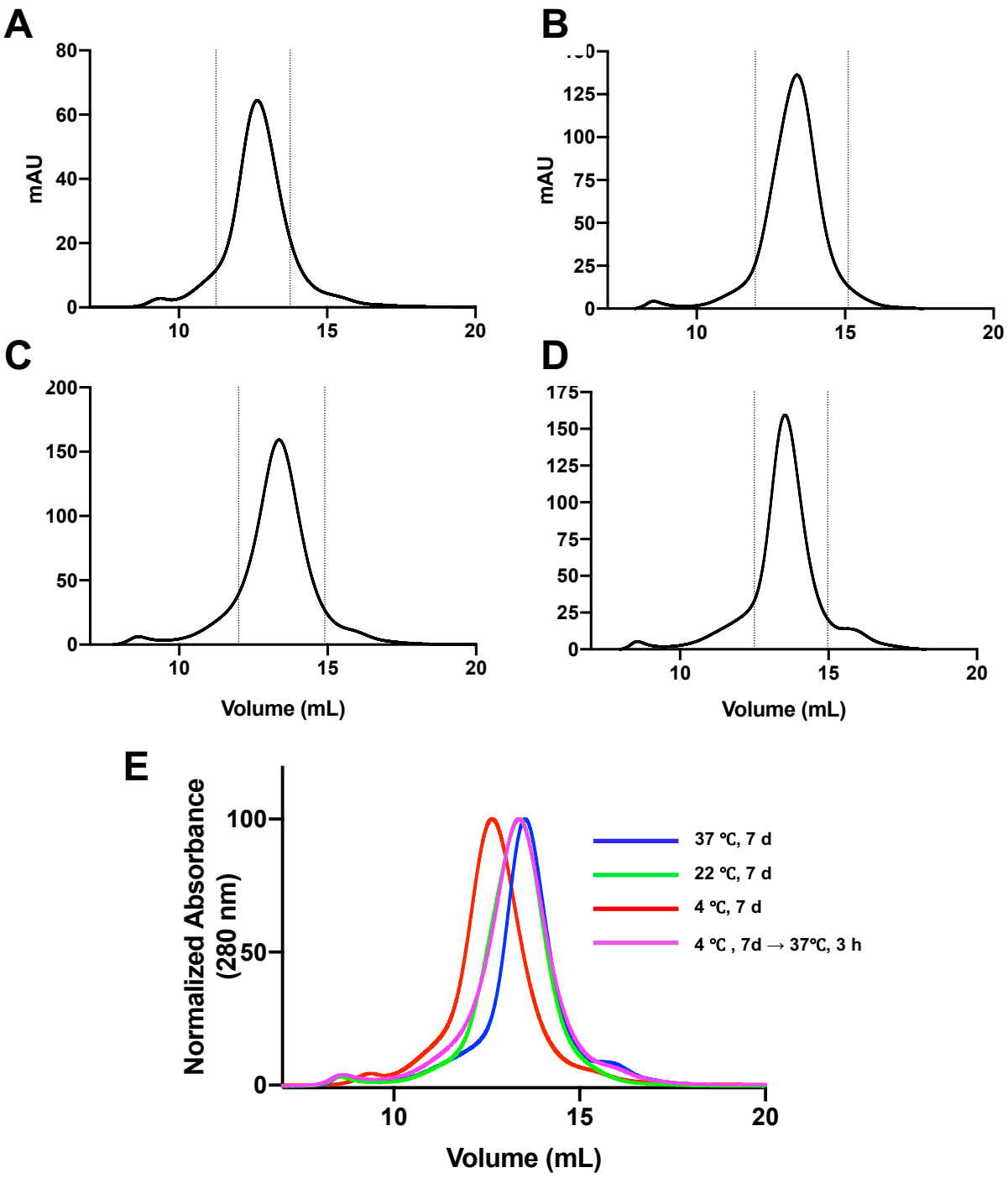

Extended Data Figure 2. Size Exclusion Chromatography of SARS-CoV-2 S ectodomain incubated at different temperatures. SEC profiles run on a Superose 6 increase 10/300 column for SARS-CoV-2 S ectodomain samples that were incubated at **(A)** 4 °C for one week, **(B)** 22 °C for one week. **(C)** 37 °C for one week, and **(D)** 4 °C for one week and moved to 37 °C for 3 hours prior to the experiment. **(E)** Overlay of SEC plots normalized to allow better visualization of peak shifts.

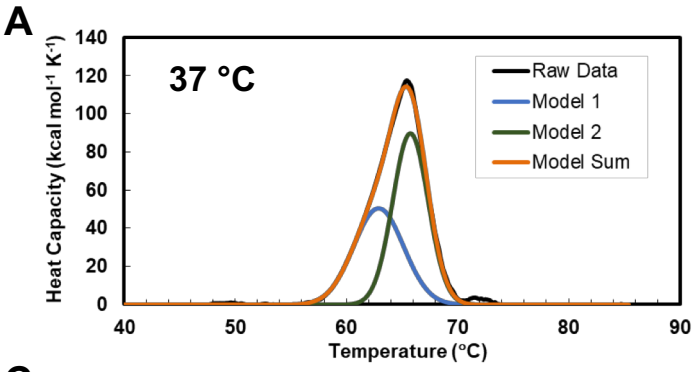

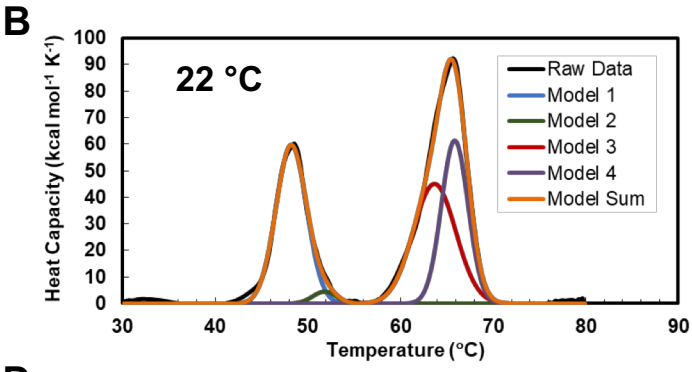

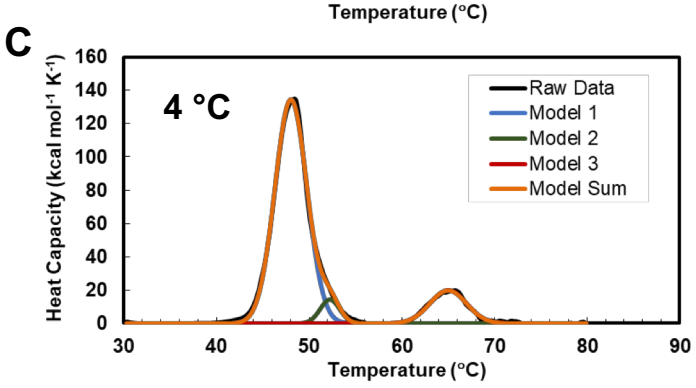

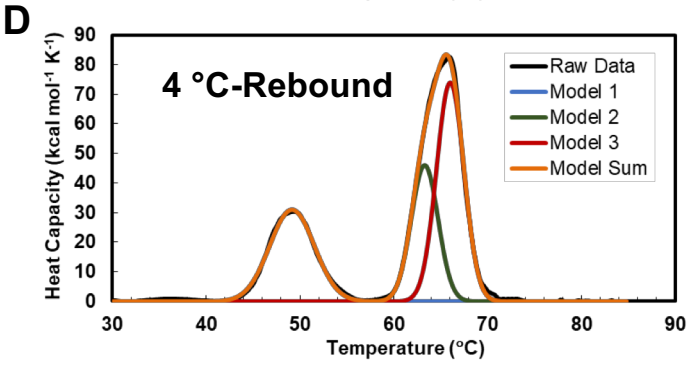

E

	Transition Peak 1		Transition Peak 2		DSC Model Fits			
	T_{onset} (°C)	T_m (°C)	T_{onset} (°C)	T_m (°C)	$T_{m,1}$ (°C)	$T_{m,2}$ (°C)	$T_{m,3}$ (°C)	$T_{m,4}$ (°C)
37 °C	N/A	**N/A**	57.5 ± 0.3	**65.5 ± 0.1**	63.2 ± 0.5	65.74 ± 0.01	N/A	N/A
22 °C	43.64 ± 0.01	**48.23 ± 0.04**	58.5 ± 0.9	**65.8 ± 0.1**	48.23 ± 0.04	51.9 ± 0.02	63.5 ± 0.3	65.92 ± 0.04
4 °C	43.0 ± 0.3	**48.41 ± 0.01**	61.1 ± 0.1	**65.1 ± 0.2**	48.02 ± 0.02	52.4 ± 0.2	65.1 ± 0.2	N/A
4 °C-Rebound	42.5 ± 0.4	**49.21 ± 0.05**	59.59 ± 0.03	**65.95 ± 0.01**	49.21 ± 0.05	63.4 ± 0.2	66.1 ± 0.1	N/A

Extended Data Figure 3. Thermostability of the SARS-CoV-2 spike ectodomain stored at different temperatures. Representative thermal denaturation profiles of the SARS-CoV-2 spike ectodomain after 1 week incubations at (**A**) 37 °C , (**B**) 22 °C, (**C**) 4 °C, and (**D**) 4 °C followed by 37 °C for 3 hours. Profiles and transition parameters (**E**) were obtained by DSC and analyzed as described in Methods. Raw data (black) was best fit with two or more Gaussian transition models ($T_{m,1\text{-}4}$) (blue, green, red, purple). The peak observed at ~65 °C was best fit with two Gaussian transition models suggesting a complex unfolding mechanism. Data shown are the mean and standard deviation from two replicate measurements.

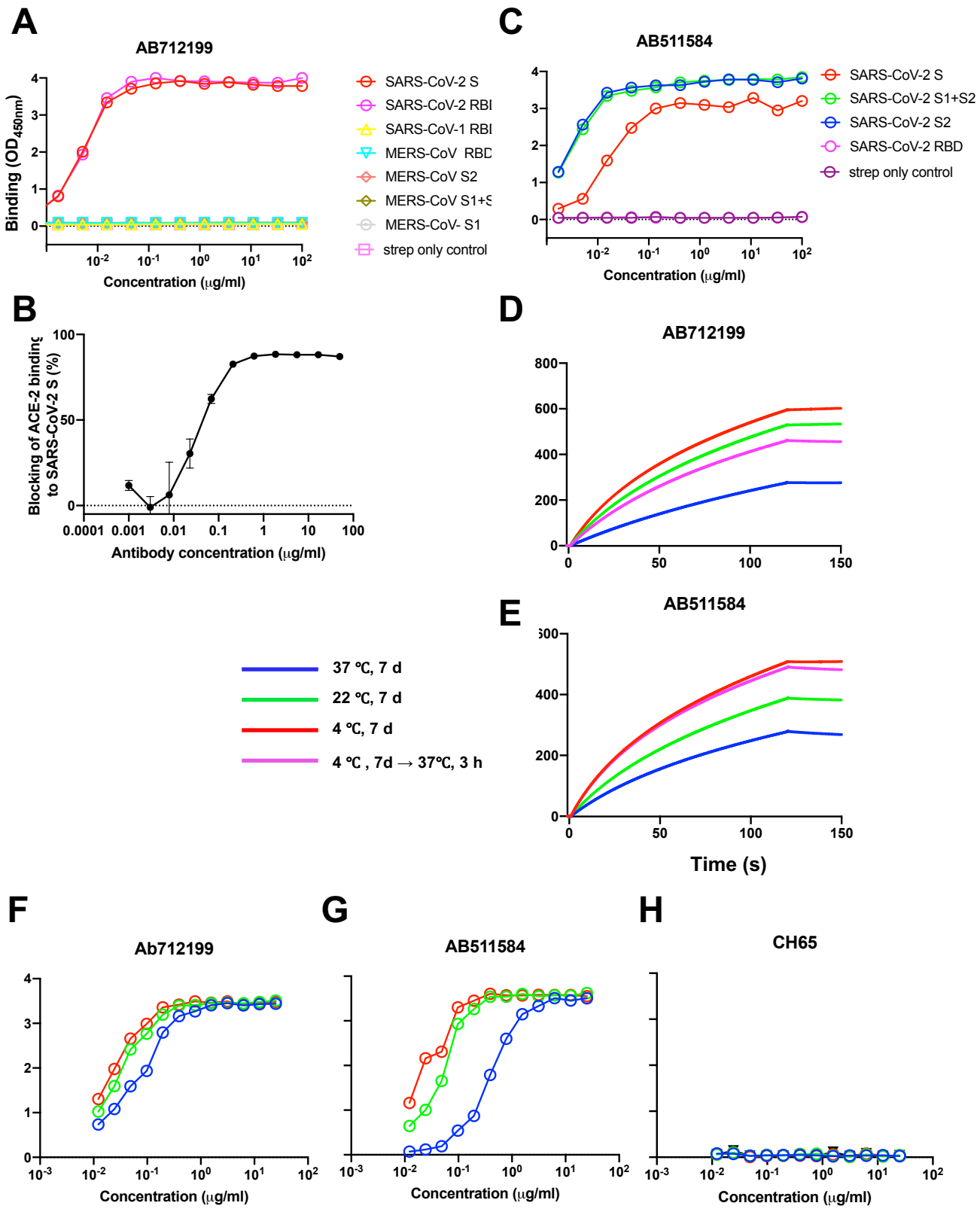
A
AB712199
Binding (OD450nm)
Concentration (μg/ml)
SARS-CoV-2 S
SARS-CoV-2 RBI
SARS-CoV-1 RBI
MERS-CoV RBD
MERS-CoV S2
MERS-CoV S1+S
MERS-CoV- S1
strep only control
C
AB511584
Concentration (μg/ml)
SARS-CoV-2 S
SARS-CoV-2 S1+S2
SARS-CoV-2 S2
SARS-CoV-2 RBD
strep only control
B
Blocking of ACE-2 binding to SARS-CoV-2 S (%)
Antibody concentration (μg/ml)
D
AB712199
E
AB511584
37 ℃, 7 d
22 ℃, 7 d
4 ℃, 7 d
4 ℃ , 7d → 37℃, 3 h
Time (s)
F
Ab712199
Concentration (μg/ml)
G
AB511584
Concentration (μg/ml)
H
CH65
Concentration (μg/ml)

Extended Data Figure 4. Antigenic response of SARS-CoV-2 S ectodomain incubated at different temperatures to antibodies elicited from convalescent patient sera. (**A**) Epitope mapping of AB712199 isolated from convalescent patient #26 that shows that the antibody binds the SARS-CoV-2 RBD region, (**B**) Blocking of ACE-2 binding to SARS-CoV-2 S ectodomain by AB712199, **(C)** Epitope mapping of AB511584 isolated from convalescent patient #26 that shows that the antibody binds the SARS-CoV-2 S2 region (**D-E**) SPR binding profiles showing binding of **(D)** RBD-directed antibody, AB712199, **(E)** S2-directed antibody, AB511584 to spike samples incubated for 1 week at either 37 °C (blue), 22 °C (green) or 4 °C (red). Binding to spike sample first incubated at 4 °C for 1 week, then moved to 37 °C for 3 hours prior to the experiment is shown in magenta. **(F-H)** ELISA binding profiles showing binding of **(F)** RBD-directed antibody, AB712199, **(G)** (middle) S2-directed antibody, AB511584, or **(H)** influenza HA-directed antibody CH65 (control) to spike samples incubated for 1 week at either 37 °C (blue), 22 °C (green) or 4 °C (red).

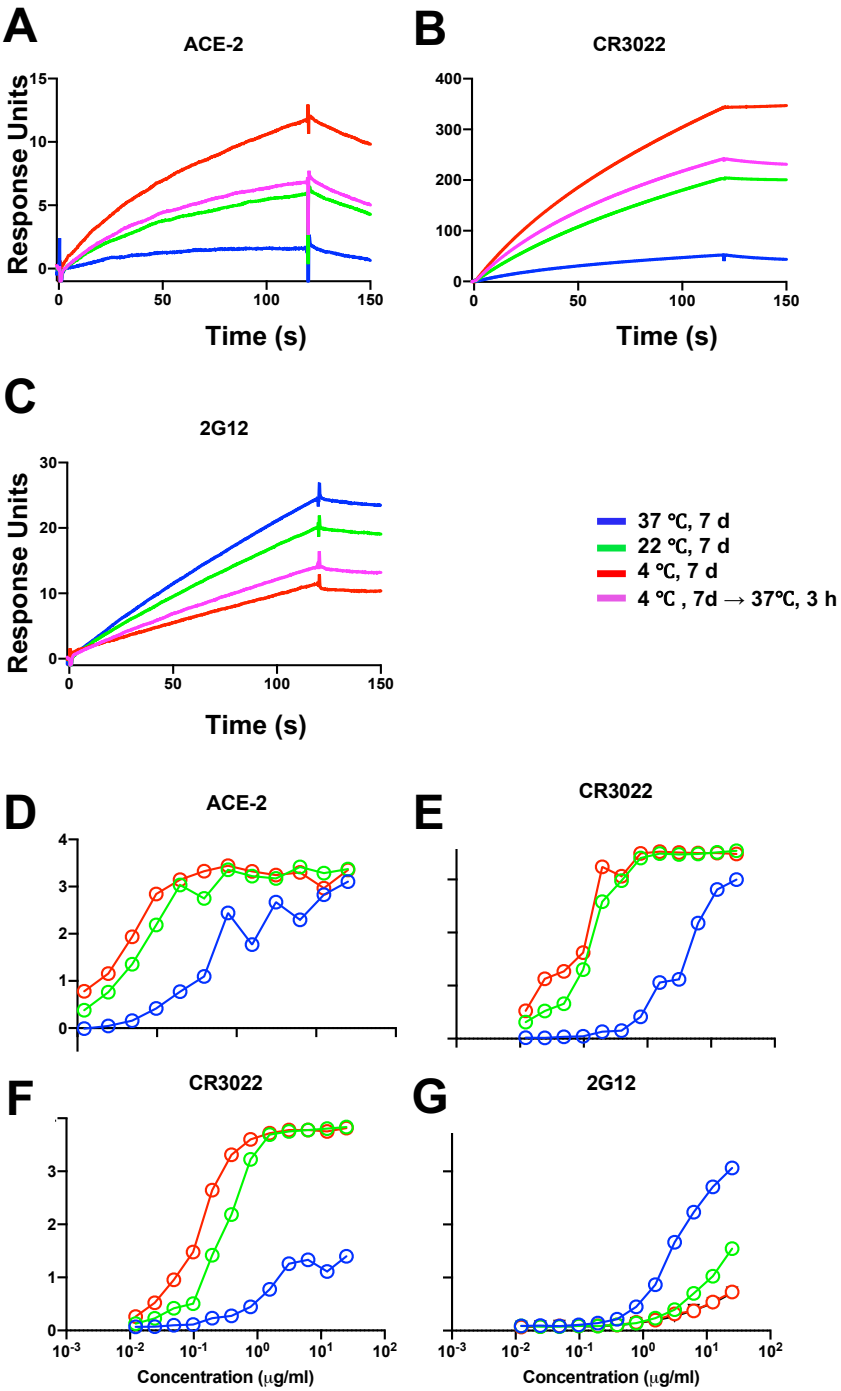

Extended Data Figure 5. Changes in antigenicity of SARS-CoV-2 S ectodomain incubated at different temperatures. (A-C) SPR profiles showing binding of **(A)** ACE-2, **(B)** RBD-directed antibody, CR3022, and **(C)** S2 glycan-directed antibody 2G12 to spike samples incubated for 1 week at either 37 °C (blue), 22 °C (green) or 4 °C (red). Binding to spike sample first incubated at 4 °C for 1 week, then moved to 37 °C for 3 hours prior to the experiment is shown in magenta. **(D-G)** ELISA binding profiles showing binding of **(D)** ACE-2, **(E)** RBD-directed antibody, CR3022, in a format where antibody was coated on the plate (see methods) and **(F)** CR3022 and **(G)** 2G12**,** in a format where spike was captured on a strep-coated plate (see methods).

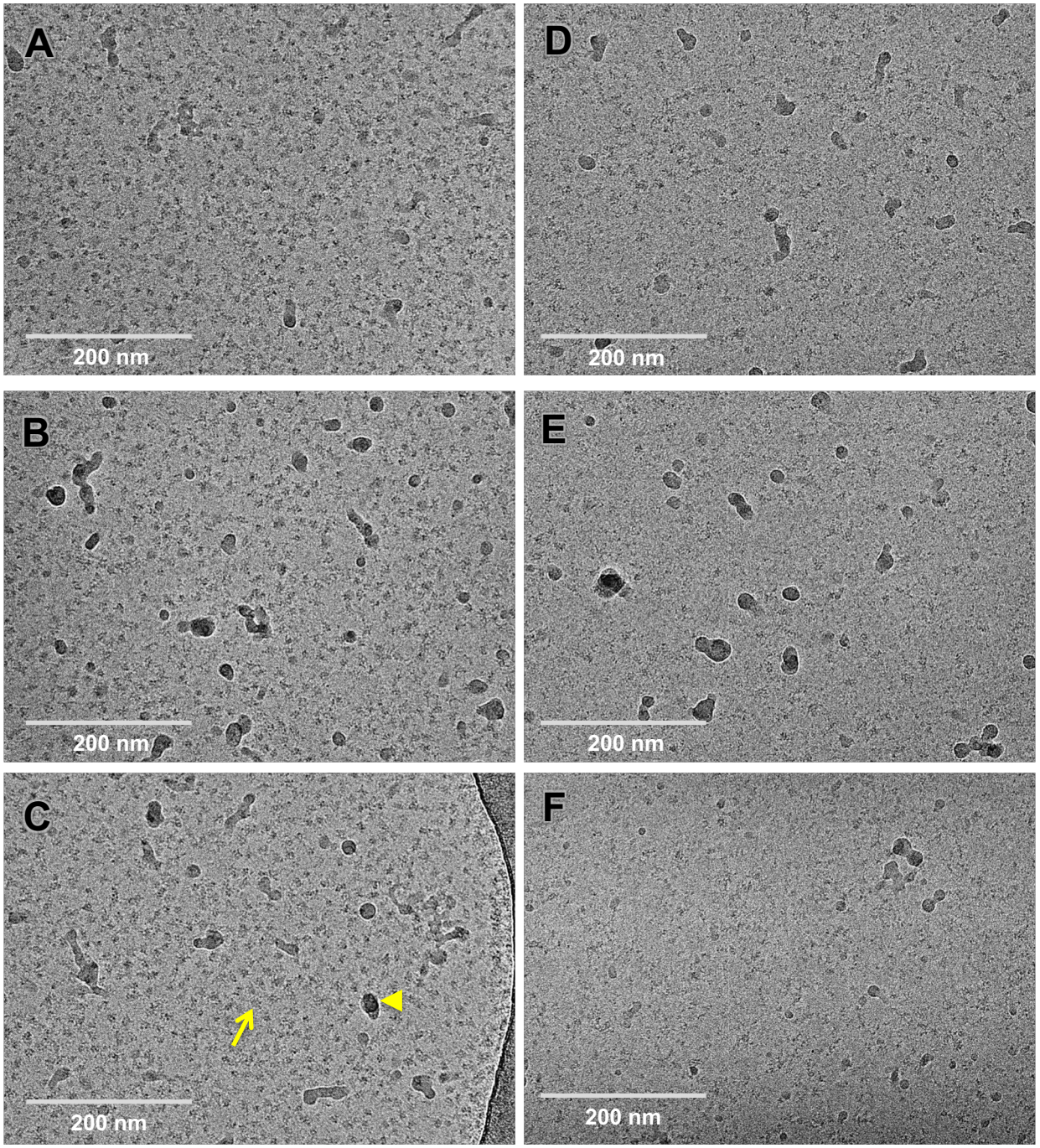

Extended Data Figure 6. Effect of SARS-CoV-2 ectodomain spike sample storage on cryo-EM specimen preparation. (**A-C**) Representative cryo-EM micrographs of a SARS-CoV-2 S ectodomain sample that was flash frozen immediately after purification and stored in -80 °C, then thawed rapidly and incubated for ~ 5 min at 37 °C immediately prior to grid preparation. Cryo-EM images are low contrast, and the desired spike particles appear as medium gray spots (*e.g.* arrow) on a light gray background. Dark gray or black spots are slight ice contamination (*e.g* arrowhead). These panels on the left show an excellent distribution of discrete spike particles. **(D-F)** Representative cryo-EM micrographs of SARS-CoV-2 S ectodomain samples that were stored for ~1 week at 4 °C prior to grid preparation. Compared to the panels of the left, these panels on the right show a sparse field-of-view with very few intact spike particles visible. A similar spike concentration (~1 mg/ml) was used to freeze all the samples. Micrographs were collected on a Titan Krios microscope with a Gatan K3 camera.

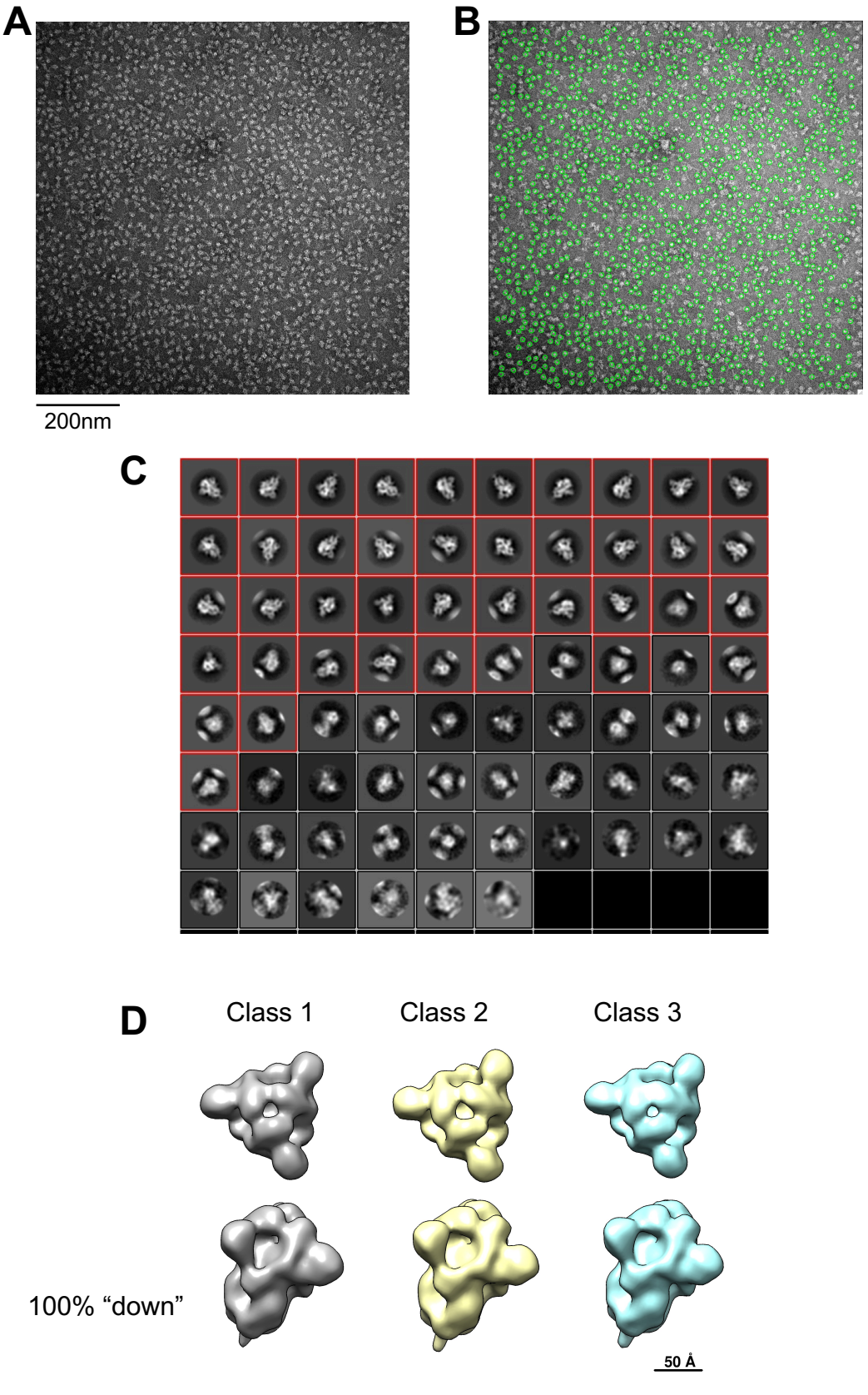
A
B
200nm
C
D
Class 1
Class 2
Class 3
100% “down”
50 Å

Extended Data Figure 7. NSEM workflow for rS2d-HexaPro. (A) Representative NSEM micrograph **(B)** Representative NSEM micrograph showing particle picks in green (C) 2D class averages; the particles in the classes marked with a red box were taken forward to the next steps on the analysis **(D)** 3D classes showing top views in the top row and side views in the bottom row. 30,000 particles were used for 3D classification. These were separated into 3 3D classes that were reconstructed using C1 symmetry. Only all-RBD-down classes were observed. Also see Supplementary Movie S1 that shows the residual movement in the RBDs despite being locked down by a RBD-to-S2 disulfide.